Translational boundaries as incipient ferrielectric domains in antiferroelectric $PbZrO_3$

Ying Liu[1,*], Ranming Niu[2,3], Andrzej Majchrowski[4], Krystian Roleder[5], Kumara Cordero-Edwards[1], Julie M. Cairney[2,3], Jordi Arbiol[1,6], Gustau Catalan[1,6,*]

[1]*Catalan Institute of Nanoscience and Nanotechnology (ICN2), Campus Universitat Autonoma de Barcelona, Bellaterra 08193, Spain*

[2]*School of Aerospace, Mechanical and Mechatronic Engineering, The University of Sydney, Sydney, N.S.W. 2006, Australia*

[3]*Australian Centre for Microscopy and Microanalysis, The University of Sydney, Sydney, N.S.W., 2006, Australia*

[4]*Institute of Applied Physics, Military University of Technology, ul. Kaliskiego 2, 00-908 Warsaw, Poland*

[5]*Institute of Physics, University of Silesia, ul. 75 Pułku Piechoty 1, 41-500 Chorzów, Poland*

[6]*Institut Català de Recerca i Estudis Avançats (ICREA), Barcelona 08010, Catalunya*

*ying.liu@icn2.cat; gustau.catalan@icn2.cat

In the archetypal antiferroelectric $PbZrO_3$, antiparallel electric dipoles cancel each other, resulting in zero spontaneous polarisation at the macroscopic level. Yet in actual hysteresis loops, the cancellation is rarely perfect and some remnant polarisation is often observed, suggesting the metastability of polar phases in this material. In this work, using aberration-corrected scanning transmission electron microscopy methods on a $PbZrO_3$ single crystal, we uncover the coexistence of the common antiferroelectric phase and a ferrielectric phase featuring an electric dipole pattern of □□□. This dipole arrangement, predicted by Aramberri *et al.* (2021) to be the ground state of $PbZrO_3$ at 0K, appears at room temperature in the form of translational boundaries. The dual nature of the ferrielectric phase, both a distinct phase and a translational boundary structure, places important symmetry constraints on its growth. These are overcome by sideways motion of the boundaries, which aggregate to form arbitrarily wide stripe domains of the polar phase embedded within the antiferroelectric matrix.

Antiferroelectrics are materials with an antiparallel but switchable alignment of electric dipoles of equal magnitude so that, in the absence of external voltage, the macroscopic net polarisation is zero [1]. Historically, $PbZrO_3$ (PZO) was the first material proposed to be antiferroelectric [2,3], and is regarded as an archetype. Its electric dipoles arrange in a □□□□ fashion (Figure 1a) [2]. For antiferroelectrics, applying a large enough electric field can rearrange the electric dipoles in the same direction, causing an antiferroelectric to ferroelectric transition identifiable by a characteristic double hysteresis loop in the polarisation as a function of the electric field [3-5]. This antipolar-to-polar switching is accompanied by giant charge storage, volume expansion and temperature drop, and hence is promising in applications in high-density capacitors [6-8], high strain transducers [9,10] and electrocaloric cooling [11,12].

Closely related to antiferroelectrics, ferrielectric phases (characterized by possessing antiparallel but uncompensated electric dipoles) have also attracted attention [13-18]. They are reported to exist in different forms and under various conditions. For example, a □□□□ dipole pattern was observed in chemically doped PZO [15,19]; in pure PZO, antiparallel electric dipoles with imbalanced magnitude were theoretically predicted to exist under an electric field [13,14], and a more complex ferrielectric structure with a □□□□□□□□ dipolar configuration was also proposed based on a combination of in-situ biasing X-ray diffraction and simulation results [17]. Interestingly, even the ground state of PZO has been proposed to be ferrielectric instead of antiferroelectric, as ab initio calculations by Aramberri *et al.* [16] suggest that a □□□ dipole pattern could be the lowest-energy state in PZO at 0K and possibly up to room temperature where, being polar, it may contribute to the open double hysteresis loop in PZO [20,21]. Yet, this ferrielectric phase has not been experimentally observed.

In this work, we uncover the existence of domains of the □□□ ferrielectric phase in PZO single crystal at room temperature. The ferrielectric periodicity is one dipole smaller than the antiferroelectric one, and therefore intercalated ferrielectric layers fulfil the role of translational boundaries (TBs). TBs are discontinuities in the periodic modulation of the antiferroelectric lattice and are intrinsic topological defects in PZO [22-24]. A schematic explanation of such translational boundaries in antiferroelectrics is shown in Figure 1b. The concept can be

understood by viewing the antipolar ordering as a square wave modulation of the polarisation, with the period of the wave being equal to four perovskite unit cells (two dipoles in one direction and two in the opposite one). The translational boundaries (blue dotted lines in Figure 1b) shift in the phase of this square wave by 1/4, 1/2 and 3/4 of the antiferroelectric (orthorhombic) unit cell, corresponding, respectively, to one, two or three pseudocubic building blocks. Domains on either side of a translational boundary are thus related by phase shifts of $\pi/2$, π, and $3\pi/2$ [23,24]. The breaking of translational symmetry implies a local disruption of the perfect dipole cancellation, and antiphase boundaries in antiferroelectrics are expected to be polar [25]. Wei *et al.* proved the polar nature of antiphase boundaries (translational boundaries with a phase shift of π) in 2014, and highlighted their potential in information storage applications [22].

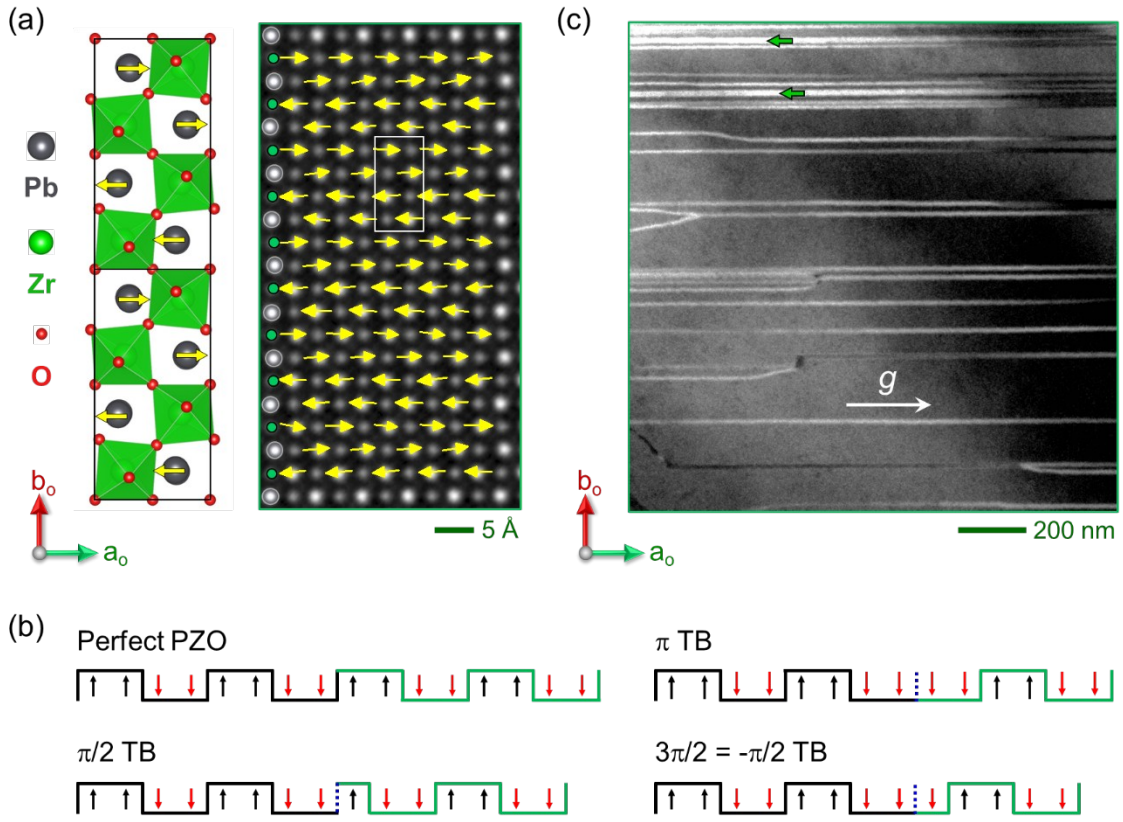

FIG. 1. (a) A structure model of PZO (two unit cells outlined by black rectangles) and a Pb displacement (Pb displacement with respect to their four nearest Zr, yellow arrows) map obtained from a STEM-HAADF image of the PZO single crystal visualized along the $\mathbf{c}_O$ axis. (b) Schematics showing electric dipole arrangements and square waves representation of the perfect PZO, PZO with $\pi/2$, π, and $3\pi/2$ TBs. Blue dotted lines denote translational

boundaries. (c) A transmission electron microscopy bright field image showing TBs observed in PZO single crystal. Green arrows indicate thicker TBs.

Ferrielectric phases and translational boundaries thus share commonalities. Both are closely related to, and can appear within, antiferroelectrics, while at the same time being polar. In this work, we show that, in pure PZO, the ferrielectric Ima2 phase predicted to be the ground state of this material, exists at room temperature forming stripe domains that also act as translational boundaries of varying thickness and with phase shifts that are integer multiples of $\pi/2$.

A single crystal of PZO was used as the sample for this study. Details of the single crystal fabrication method are provided elsewhere [26]. Electron-transparent lamellae were cut from the crystal using focussed ion beam lithography. The lamellae were heated up to 250 ˚C and cooled down to favour the nucleation of different domains. Heated up to a lower temperature such as 150 ˚C or 200 ˚C can also cause the nucleation of new ferrielectric domains close to ferroelastic domain walls (figure S1 in the supplementary materials), suggesting that mechanical strain may lower the barrier for their formation, consistent with their extended presence in epitaxial thin films [27].

The samples show the expected antiferroelectric structure of PZO (Figure 1a), but also extended planar structures (Figure 1c). These are similar to those observed by Wei *et al*. [22], who identified them as π translational boundaries, i.e. boundaries that change the phase of the dipole arrangement by a factor of π. We found, however, that the linear structures in the sample can have different thicknesses. Green arrows have been added in Figure 1c to mark some thicker ones. Further atomic-scale investigations of these stripe-like features, displayed in Figures 2 - 4, show that they are in fact ferrielectric domains that act de facto as translational boundaries with different phase angles multiple of $\pi/2$.

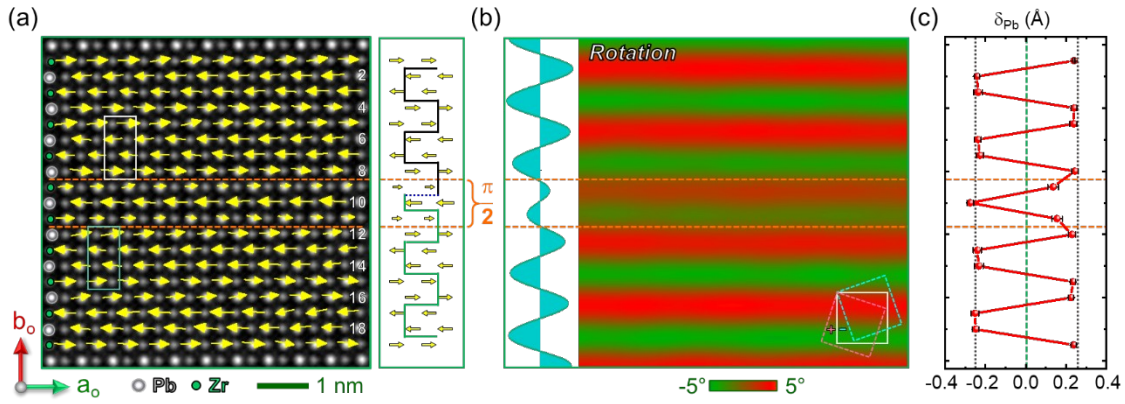

FIG. 2. (a) A Pb displacement map superimposed on the corresponding STEM-HAADF image showing a TB separating regions with π/2 difference in phase (along $\mathbf{b}_O$ direction). (b) The GPA lattice rotation map of (a). The blue inset curve is an intensity profile of the lattice rotation map. (c) The Pb displacement curve by averaging rows from 1 to 19. Error bars, standard deviation. Black dotted lines, Pb displacement in ideal antiferroelectric PZO.

Figure 2a displays a scanning transmission electron microscopy high angle annular dark field (STEM-HAADF) image of the thinnest translational boundaries found in the PZO single crystal. Pb displacements (δ_{Pb}) with respect to their four nearest Zr were extracted using Python with the "Atomap" library [28]. The obtained δ_{Pb} map was superimposed on the corresponding STEM-HAADF image. From the δ_{Pb} map, a disturbance of antiferroelectric order can be observed. Electric dipoles arrange in the □□□□□□□□ manner, where an upward dipole is missed, and the single unpaired dipole is larger in magnitude. On both sides of this dipole, the antiferroelectric domains have a phase difference of π/2 and a relative shift of 1/4 orthorhombic unit cells (i.e., one perovskite unit cell) along the orthorhombic **b** direction. We henceforth identify this ferrielectric structure as a π/2 TB.

We have also examined the lattice rotations by means of Geometric Phase Analysis (GPA) [29,30] on the atomic resolution STEM-HAADF images. GPA is a method to determine lattice strain and rotation from high-resolution images [31,32]. A GPA lattice rotation map from Figure 2a is shown in Figure 2b. The rotation angle at the TB region and its modulation period are smaller than in other upper and lower regions. The intensity profile indicates this trend. Based on this characteristic in GPA, it is possible to identify the TB even without a δ_{Pb} map. It is also to be noted that GPA gives precise strain or lattice rotation values when analyzing long-range

continuous strain. AFE PZO and TBs show short-range lattice modulations: the rotation angles change abruptly between neighbouring lattices and the corresponding values are therefore discrete. When applying GPA to PZO, the resulting lattice rotation map is sinusoidal-like (Figure 2b), because GPA defines lattice rotation at each pixel and its intrinsic averaging effect [33]. Even so, our results show the effectiveness of the GPA in determining the short-range modulation period and amplitude, and locating the TBs.

Quantitative analysis also shows that the magnitude of the middle unpaired electric dipole of the TB is bigger than the two satellite dipoles on either side, i.e., the dipolar structure is □□□. This means that, though the internal symmetry of the π/2 translational boundary is polar, its net polarisation can be positive, negative, or zero depending on the relative difference between the central dipole and the sum of the two satellites. Moreover, we find that this relative ratio can change continuously within the same TB. For example, on the far left of the TB of Figure 2a, the middle δ_{Pb} (0.25 Å) is smaller than the sum of the satellite dipoles (-0.17 Å and -0.21 Å, respectively), while on the far right of the TB, the middle dipole (δ_{Pb}, 0.31 Å) is bigger than the sum of the two satellites (δ_{Pb}, -0.07 Å and -0.15 Å, respectively).

In fact, despite the TB unit cell being polar, we find that the average polarisation is close to zero. The averaged δ_{Pb} plot as a function of the atomic rows is shown in Figure 2c. The middle δ_{Pb} (0.275 Å) is a little bigger than that in the antiferroelectric region and in the ideal PZO model (black dotted lines), while the satellite δ_{Pb} (average values of 0.135 Å and 0.155 Å) are much smaller than the middle δ_{Pb}, but the sum of the two (0.135 + 0.155 = 0.290 Å) is almost equal the antiparallel displacement of the central dipole (0.275 Å). The conclusion from this analysis is that the TB can change its internal polarisation from positive to negative or even zero while still preserving the relative sign of the internal displacements, i.e. modulating only their relative magnitude. This is a qualitative difference with respect to ferroelectrics, for which inverting the sign of polarisation requires inverting the sign of the atomic displacements within the unit cell. The ability to modulate the sign of the polarisation without having to overcome a discrete energy barrier means that the internal polarisation of the TBs can adapt to local variations in electric fields.

In addition to the π/2 TB, we have also observed TBs with two and three ▯⃗▯ dipole units (Figures 3a, 3b). By extrapolating the antiferroelectric domains across these regions, we see that the square waves that represent the antipolar modulation on both sides of the TBs shift by a period difference of 1/2 (Figure 3a) and 3/4 (Figure 3b), respectively, so these are TBs with phase differences of π and 3π/2. Translational boundaries with four or more ▯⃗▯ dipole units have never been considered in previous research, yet they are also observed in our experiment. Figures 3c - 3e show the superimposed STEM-HAADF micrographs + δ_{Pb} maps and GPA lattice rotation maps for wider TBs. From these images, four (Figure 3c), five (Figure 3d) and seven (Figure 3e) π/2 TB structural units can be determined.

The formation of π/2, π and 3π/2 TBs is theoretically justified: they are topologically inevitable whenever adjacent antiferroelectric domains nucleate at atomic sites separated by a non-integer multiple of 4 perovskite unit cells along the polar-modulation direction. They are topologically protected because, to eliminate a TB, it is necessary to change the phase (and thus rearrange the dipoles) of at least one of the adjacent antiferroelectric domains. In contrast, TBs with a phase difference of 2π (equal to four π/2 TBs), such as in Figure 3c, do not enjoy such topological protection as there is no phase difference between the adjacent domains. Put another way: 4 ▯⃗▯ dipole units can be replaced by 3 ▯▯▯▯ antiferroelectric dipole units without disturbing the translational symmetry of the adjacent domains. Likewise, five or seven π/2 TB can, in theory, be replaced by one antiferroelectric structural unit plus one or three π/2 TB structural units, which would in principle lower the crystal's energy if the antiferroelectric state was the ground state.

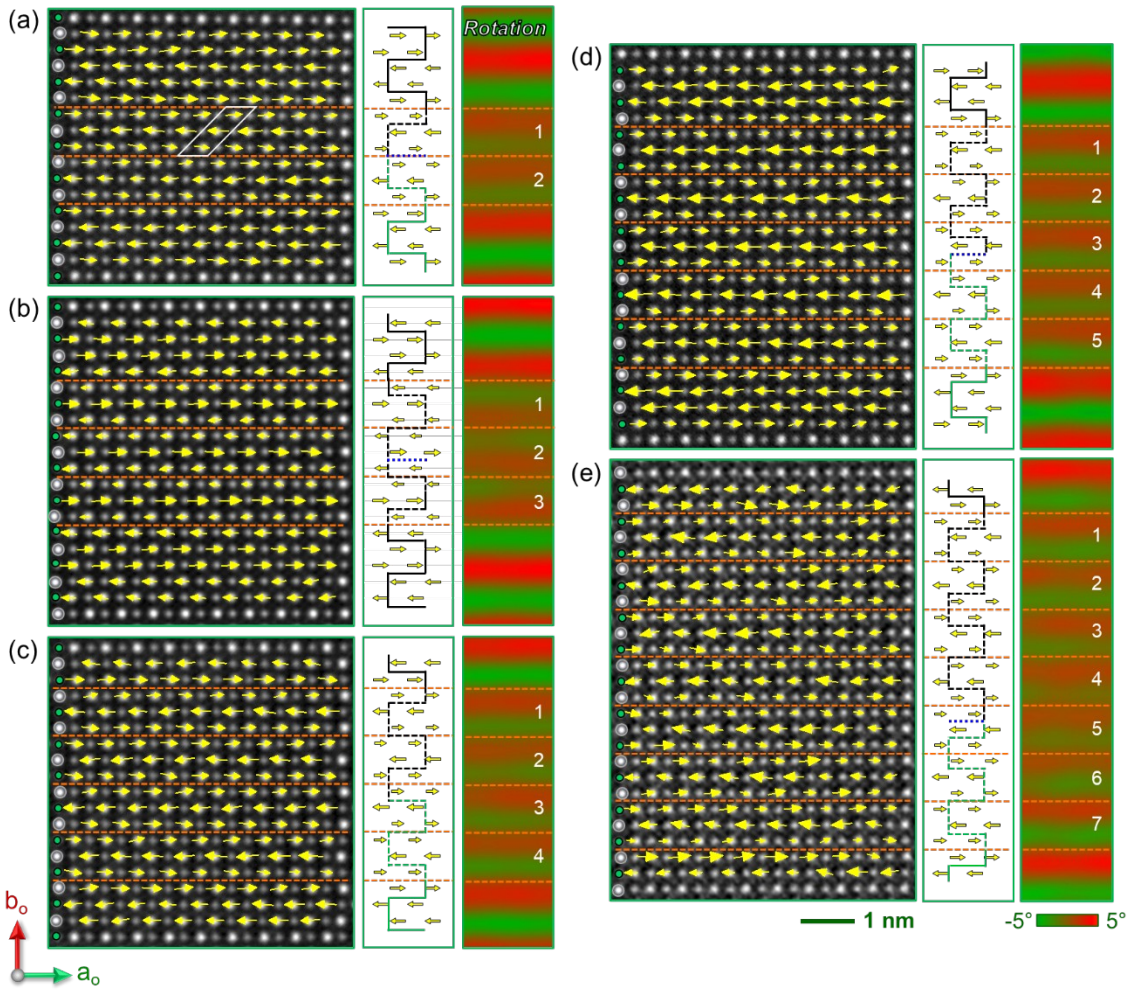

FIG. 3. TBs or ferrielectric phases observed in $PbZrO_3$ single crystal with (a) two, (b) three, (c) four, (d) five and (e) seven □□□ structural units, corresponding to phase differences of π, 3π/2, 0, π/2 and 3π/2, respectively. A ferrielectric structural unit is outlined by a white parallelogram in (a). A superimposed STEM-HAADF image + Pb map, a Pb displacement schematic and a GPA lattice rotation map are included in each panel. In Pb displacement schematics, the square waves are extended from outside (solid lines) to inside (dashes lines) of TBs until they meet, showing phase differences of π, 3π/2, 0, π/2, 3π/2, respectively. TBs, blue dotted lines.

At this point, then, it becomes necessary to reexamine whether these structures should still be regarded as translational boundaries. They can also be viewed as domains of a ferrielectric phase (□□□) embedded within the antiferroelectric matrix (□□□□). Since the thicker stripes are not a topological necessity, their existence suggests that the free energy of the ferrielectric phase must be sufficiently low to be at least locally stable at room temperature. Indeed, the three-dipole

arrangement of the TBs is the same unit cell proposed by Aramberri *et al.* [16] as the theoretical ground state of PZO.

The dual nature of the FiE phase (both a separate phase and a translational boundary structure) also means that its growth is topologically hindered by the translational symmetry of AFE matrix. Nucleating new FiE domains at room temperature is nevertheless possible: we have observed it to happen as boundaries around small needle-like antiferroelectric domains (yellow arrow in Figure 4), typically nucleating near lattice discontinuities such as interfaces or twin walls (supplementary figure S1). Note that the continuity of the AFE matrix dictates that the two TBs that bound such needles must have a combined phase difference that is an integer multiple of 2π. The electron-beam-induced motion of the FiE domains was also observed (blue arrows in Figure 4), showing that the ferrielectric phase is sensitive to electric fields [27].

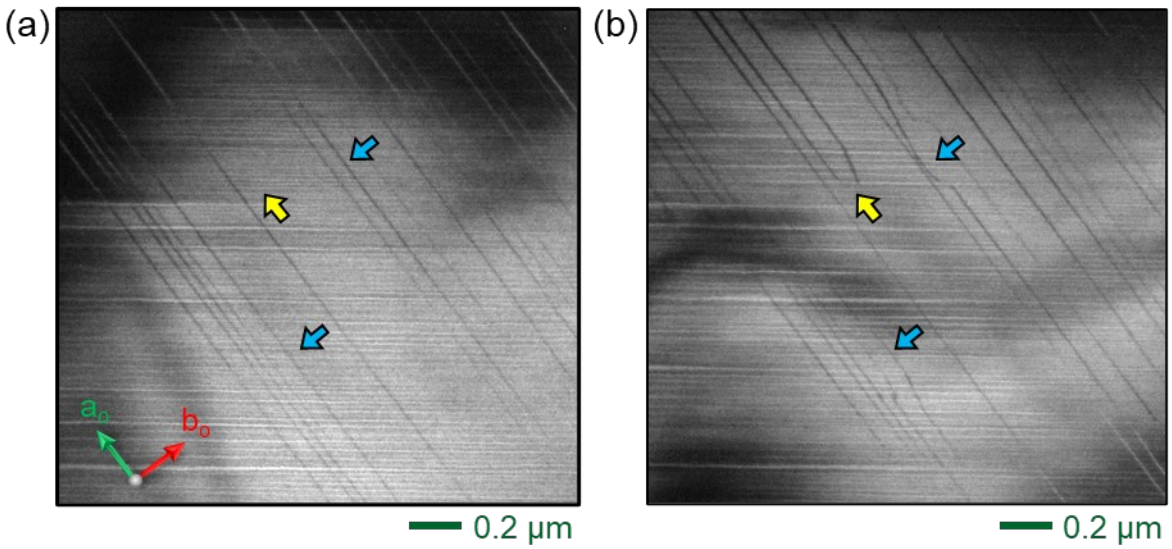

FIG. 4. Nucleation and movement of FiE regions at room temperature, induced by sustained electron irradiation inside the TEM. The yellow arrow shows a new FiE stripe as the TB around a needle-like AFE domain. The upper blue arrows show the FiE stripe movements.

In order to fully characterize the ferrielectric unit cell, it is necessary to determine its oxygen positions. In STEM-HAADF images, only Pb and Zr can be observed. Instead, we turn to STEM integrated differential phase contrast (iDPC) imaging, which is sensitive to light elements [34]

and can image oxygens in perovskite oxides [35]. The results for a π/2 and π TB are shown in Figures 5a and 5b, respectively. A primitive cell is outlined using a white parallelogram in Figure 54a. Along the $\mathbf{a}_O$ direction, all horizontal oxygen chains are slightly rippled, and tilt in opposite directions on both sides of the biggest Pb displacements (central dipole in the TB structural units). Along the $\mathbf{b}_O$ direction, the tilting pattern is **/ - | -**, that is, clockwise, straight, anticlockwise, with the central (bigger) dipole coinciding with the untilted oxygen chain and showing the characteristic anti-correlation between tilts and polarisations in perovskites. A unit cell was outlined by a white rectangle in Figure 5b. The structural model built according to experimental results and optimised using density functional theory is shown in Figure 5c (more details in Supplementary materials, Figure S2). The space group of the optimised structure is also Ima2, the same as that reported in Ref. [16].

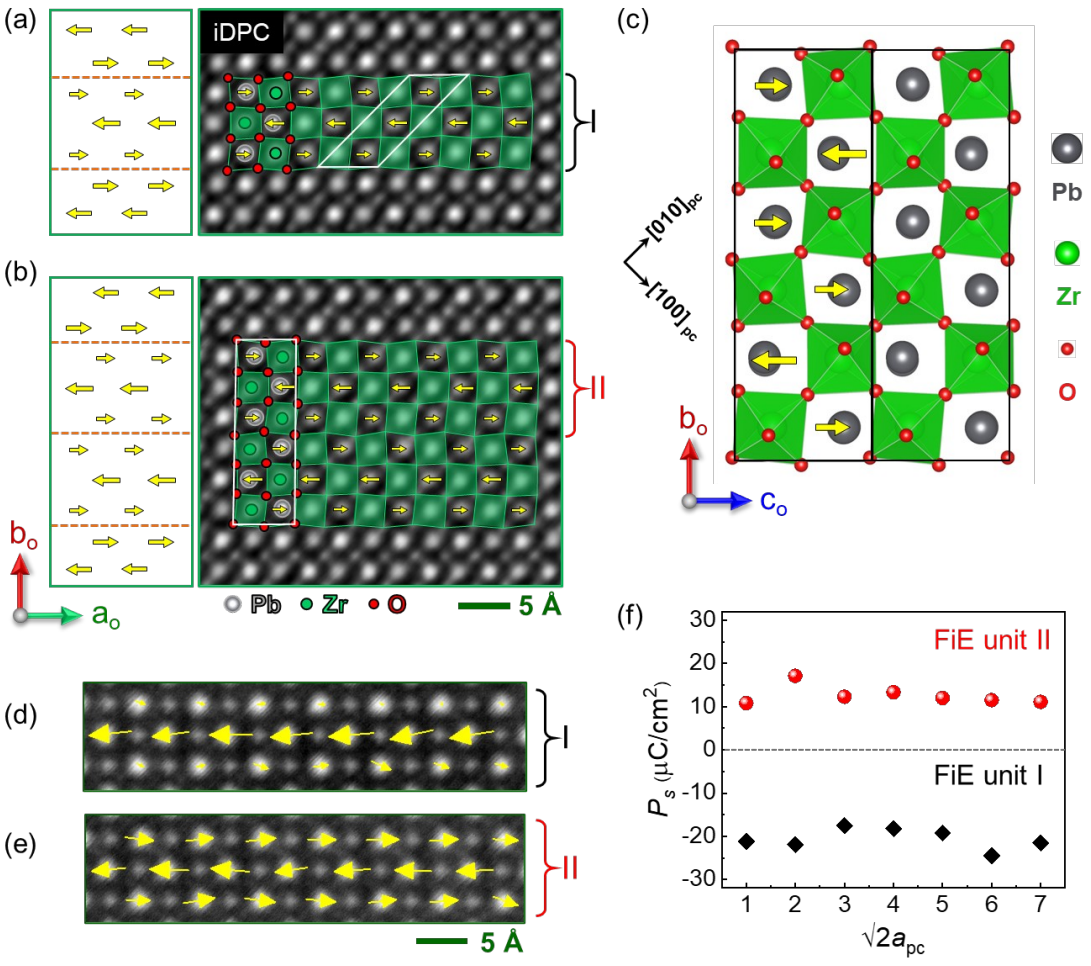

FIG. 5. (a, b) STEM-iDPC images showing Pb, Zr and O distribution at π/2 and π TBs, respectively. (c) The ferrielectric PZO model. Two unit cells are outlined using black rectangles. (d) The STEM-HAADF image of the same FiE unit as that labelled "I" in (a). (e) The STEM-HAADF image of the same FiE unit as that labelled "II" in (b). (f) Unit cell scale spontaneous polarisation that was calculated based on the Pb, Zr and O positions in the corresponding iDPC images.

The HAADF images and superimposed δ_{Pb} map corresponding to the FiE unit I and II labelled in Figures 5a and 5b are shown in Figures 5d and 5e, respectively. By extracting Pb, Zr and O positions from iDPC images in Figures 5a and 5b, the polarisation was quantitatively calculated using the Born effect charge method where $P_s = V^{-1} \sum_i {}_iZ_i$ and shown in Figure 5f. The FiE unit I shows positive and the FiE unit II shows negative polarisations, despite both having the same orientation of the central dipoles (see Figures 5d and 5e). This result provides further evidence that the sign of polarisation can change without switching the sign of Pb displacements. The Born effect charge used in the P_s calculation is from Ref. [22].

In terms of functionalities, since the FiE domains (TBs) are polar, and therefore piezoelectric and capable of optical second harmonic generation. They also may contribute to the small remnant polarisation at 0V often reported in the double hysteresis loops of PZO [20,21,36,37] but, given the uncertainty about the magnitude of their polarisation, it is hard to quantify their contribution. The observation that polarisation can easily vary in magnitude and sign within ferrielectric domains also suggests that these structures have high dielectric susceptibility and increasing their concentration may therefore be beneficial for capacitor applications. Since the FiE phase can be generated anytime the AFE phase is freshly nucleated, repeated field-induced switching of the antiferroelectric may result in a progressive accumulation of polar domains. This would manifest as an "anti-fatigue", whereby the remnant polarisation increases with the number of switching cycles; this is the opposite of ferroelectric fatigue, whereby polarisation decreases with repeated switching. This "reverse fatigue" phenomenon of antiferroelectrics has been observed [38].

Ferrielectrics share some of the properties of antiferroelectrics (they are antipolar lattices that can be switched into a homogeneous polar state by application of an external voltage) and some of those of ferroelectrics (remnant polarisation, piezoelectricity and so forth). As such, they are an exciting prospect for new concepts in multifunctional devices combining both functionalities,

e.g. energy storage (antiferroelectric) and data storage (ferroelectric). Our work on single crystals suggests that $PbZO_3$ is energetically close to being ferrielectric, with the FiE phase showing up as translational boundaries that aggregate to form wider stripe domains where the phase difference is larger than $3\pi/2$, the maximum topological value [22]. Here, topological protection acts as a double-edged sword: it guarantees the existence of FiE domains in the form of translational boundaries, but it complicates their growth precisely because of its impact on the translational symmetry of the AFE matrix. Overcoming this obstacle will require either finding a composition or strain state where the FiE phase nucleates at a higher temperature than the AFE one, or else repeated switching in the hope that the progressive accumulation of TBs tilts the energy balance in favour of a homogeneous ferrielectric phase.

ACKNOWLEDGEMENTS

This project has received funding from the European Union's Horizon 2020 research and innovation program under grant agreement N° 766726 (TSAR), in addition to Grant PID2019-108573GB-C21 funded by MCIN/AEI/10.13039/501100011033. ICN2 acknowledges funding from Generalitat de Catalunya 2017 SGR 327. ICN2 is supported by the Severo Ochoa program from Spanish MINECO (Grant No. SEV-2017-0706) and is funded by the CERCA Programme / Generalitat de Catalunya. YL acknowledges the BIST Postdoctoral Fellowship Programme (PROBIST) funded by the European Union's Horizon 2020 research and innovation programme under the Marie Sklodowska-Curie grant agreement No. 754510. KC and AM acknowledge funding by the National Science Centre, Poland, grant number 2020/37/B/ST3/02015. The authors are grateful for the scientific and technical support from the Australian Centre for Microscopy and Microanalysis (ACMM) as well as the Microscopy Australia Node at the University of Sydney. Thanks Prof. Jorge Íñiguez and Dr. Hugo Aramberri from the Luxembourg Institute of Science and Technology (LIST) for the discussion of the space group and Glazer notation of the ferrielectric phase. Thanks to PhD student Ran Xu, from University Paris-Saclay, CentraleSupelec, CNRS, Laboratoire SOMS, for assistance in the geometric optimisation of FiE PZO unit cell using density functional theory.

REFERENCES

[1] C. Kittel, Phys. Rev. **82**, 729 (1951).

[2] E. Sawaguchi, H. Maniwa, and S. Hoshino, Phys. Rev. **83**, 1078 (1951).

[3] G. Shirane, E. Sawaguchi, and Y. Takagi, Phys. Rev. **84**, 476 (1951).

[4] X. Tan, C. Ma, J. Frederick, S. Beckman, and K. G. Webber, J. Am. Ceram. Soc. **94**, 4091 (2011).

[5] P. Vales-Castro, M. Vellvehi, X. Perpiñà, J. M. Caicedo, X. Jordà, R. Faye, K. Roleder, D. Kajewski, A. Perez-Tomas, E. Defay, and G. Catalan, Adv. Electron. Mater. **7**, 2100380 (2021).

[6] A. Chauhan, S. Patel, R. Vaish, and C. R. Bowen, Materials **8**, 8009 (2015).

[7] Z. Liu, T. Lu, J. Ye, G. Wang, X. Dong, R. Withers, and Y. Liu, Adv. Mater. Technol. **3**, 1800111 (2018).

[8] C. A. Randall, Z. Fan, I. Reaney, L.-Q. Chen, and S. Trolier-McKinstry, J. Am. Ceram. Soc. **104**, 3775 (2021).

[9] W. Y. Pan, C. Q. Dam, Q. M. Zhang, and L. E. Cross, J. Appl. Phys. **66**, 6014 (1989).

[10] S.-E. Park, M.-J. Pan, K. Markowski, S. Yoshikawa, and L. E. Cross, J. Appl. Phys. **82**, 1798 (1997).

[11] R. Pirc, B. Rožič, J. Koruza, B. Malič, and Z. Kutnjak, EPL (Europhysics Letters) **107**, 17002 (2014).

[12] P. Vales-Castro, R. Faye, M. Vellvehi, Y. Nouchokgwe, X. Perpiñà, J. M. Caicedo, X. Jordà, K. Roleder, D. Kajewski, A. Perez-Tomas, E. Defay, and G. Catalan, Phys. Rev. B **103**, 054112 (2021).

[13] P. Tolédano, and M. Guennou, Phys. Rev. B **94**, 014107 (2016).

[14] P. Tolédano, and D. D. Khalyavin, Phys. Rev. B **99**, 024105 (2019).

[15] Z. Fu, X. Chen, Z. Li, T. Hu, L. Zhang, P. Lu, S. Zhang, G. Wang, X. Dong, and F. Xu, Nat. Commun. **11**, 3809 (2020).

[16] H. Aramberri, C. Cazorla, M. Stengel, and J. Íñiguez, Npj Comput. Mater. **7**, 196 (2021).

[17] R. G. Burkovsky, G. A. Lityagin, A. E. Ganzha, A. F. Vakulenko, R. Gao, A. Dasgupta, B. Xu, A. V. Filimonov, and L. W. Martin, Phys. Rev. B **105**, 125409 (2022).

[18] L. Qiao, C. Song, Q. Wang, Y. Zhou, and F. Pan, ACS Appl. Nano Mater. **5**, 6083 (2022).

[19] T. Ma, Z. Fan, B. Xu, T. H. Kim, P. Lu, L. Bellaiche, M. J. Kramer, X. Tan, and L. Zhou, Phys. Rev. Lett. **123**, 217602 (2019).
[20] L. Pintilie, K. Boldyreva, M. Alexe, and D. Hesse, J. Appl. Phys. **103**, 024101 (2008).
[21] M. Guo, M. Wu, W. Gao, B. Suna, and X. Lou, J. Mater. Chem. C **7**, 617 (2019).
[22] X. K. Wei, A. K. Tagantsev, A. Kvasov, K. Roleder, C. L. Jia, and N. Setter, Nat. Commun. **5**, 3031 (2014).
[23] I. Rychetsky, W. Schranz, and A. Troster, Phys. Rev. B **104**, 224107 (2021).
[24] X. K. Wei, C. L. Jia, K. Roleder, and N. Setter, Mater. Res. Bull. **62**, 101 (2015).
[25] G. Catalan, J. Seidel, R. Ramesh, and J. F. Scott, Rev. Mod. Phys. **84**, 119 (2012).
[26] J.-H. Ko, M. Górny, A. Majchrowski, K. Roleder, and A. Bussmann-Holder, Phys. Rev. B **87**, 184110 (2013).
[27] R.-J. Jiang, Y. Cao, W.-R. Geng, M.-X. Zhu, Y.-L. Tang, Y.-L. Zhu, Y. Wang, F. Gong, S.-Z. Liu, Y.-T. Chen, J. Liu, N. Liu, J.-H. Wang, X.-D. Lv, S.-J. Chen, and X.-L. Ma, Nano Lett., **23**, 1522 (2023).
[28] M. Nord, P. E. Vullum, I. MacLaren, T. Tybell, and R. Holmestad, Adv. Struct. Chem. Imaging **3**, 9 (2017).
[29] M. J. Hytch, E. Snoeck, and R. Kilaas, Ultramicroscopy **74**, 131 (1998).
[30] Y. Liu, Y. J. Wang, Y. L. Zhu, C. H. Lei, Y. L. Tang, S. Li, S. R. Zhang, J. Li, and X. L. Ma, Nano Lett. **17**, 7258 (2017).
[31] Y. L. Tang, Y. L. Zhu, X. L. Ma, A. Y. Borisevich, A. N. Morozovska, E. A. Eliseev, W. Y. Wang, Y. J. Wang, Y. B Xu, Z. Zhang, S. J. Pennycook, Science **348**, 547 (2015).
[32] Y. L. Tang, Y. L. Zhu, Y. Liu, Y. J. Wang, and X. L. Ma, Nat. Commun. **8**, 15994 (2017).
[33] J. L. Rouvière, and E. Sarigiannidou, Ultramicroscopy **106**, 1 (2005).
[34] I. Lazić, E. G. T. Bosch, and S. Lazar, Ultramicroscopy **160**, 265 (2016).
[35] Y. Liu, R.-M. Niu, S. D. Moss, P. Finkel, X. Z. Liao, and J. M. Cairney, J. Appl. Phys. **129**, 234101 (2021).
[36] J. Ge, D. Remiens, X. Dong, Y. Chen, J. Costecalde, F. Gao, F. Cao, and G. Wang, Appl. Phys. Lett. **105**, 112908 (2014).
[37] K. Boldyreva, D. Bao, G. L. Rhun, L. Pintilie, M. Alexe, and D. Hesse, J. Appl. Phys. **102**, 044111 (2007).
[38] P. Mohapatra, D. D. Johnson , J. Cui, and X. Tan, J. Mater. Chem. C **9**, 15542 (2021).